TEMPERATURE DEPENDENCE OF THE THERMOREFLECTANCE COEFFICIENT OF GOLD USING A PHASE-LOCKED SINGLE-POINT MEASUREMENT APPROACH

Approved by:

Dr. Peter Raad
Professor

Dr. Ali Beskok
Professor

Dr. David Willis
Associate Professor

TEMPERATURE DEPENDENCE OF THE THERMOREFLECTANCE COEFFICIENT OF GOLD USING A PHASE-LOCKED SINGLE-POINT MEASUREMENT APPROACH

A Thesis Presented to the Graduate Faculty of the

Lyle School of Engineering

Southern Methodist University

in

Partial Fulfillment of the Requirements

for the degree of

Master of Science in Mechanical Engineering

with a

Major in Mechanical Engineering

by

Assaad El Helou

(B.E., Mechanical Engineering, American University in Beirut, Lebanon)

May 20, 2017

ACKNOWLEDGMENTS

This work could not have been accomplished without the help and constant support of my advisor, Prof. Raad, who guided my efforts and provided me with a major source of knowledge and expertise in the field. I am also grateful to TMX Scientific for granting me access to their facility and to its Research team, especially Dr. Komarov, who was always available for assistance and feedback while working on my experimental setup. I would like to acknowledge the help Prof. Beskok in providing the needed access and training in the micro-fabrication clean room to work on the samples, and all of his colleagues in the Department of Mechanical Engineering at SMU that contributed to my academic and research journey.

El Helou, Assaad (B.E., Mechanical Engineering, American University in Beirut, Lebanon)

Temperature Dependence of the Thermoreflectance Coefficient
of Gold using a Phase-Locked Single-Point Measurement Approach

Advisor: Dr. Peter Raad
Master of Science in Mechanical Engineering degree conferred May 20, 2017
Thesis completed May 4, 2017

Thermoreflectance has become a widely accepted and reliable temperature metrology tool that measures at sub-micron resolutions. However, the accuracy of the technique in reporting absolute temperatures relies on the calibration method and on the linear coefficient, C_{TR}, relating the temperature to the reflectance change. This study investigates the linear assumption by measuring C_{TR} between 25°C and 100°C. A high precision optical setup is assembled to measure the coefficient of thermo-reflectance of gold using a single-point phase-locked technique. The measurements of C_{TR} are validated by two CCD measurement setups with thermoelectric heating and in-situ self heating. The results show that the coefficient is not constant as previously assumed, but gradually drops from $4 \times 10^{-4} K^{-1}$ to $3 \times 10^{-4} K^{-1}$ as the calibration temperature increases from 25°C to 100°C. The effect of this deviation from the linear assumption's on the accuracy of microscopy tools is an error in excess of 10°C over the studied temperature range. The techniques used in this study also serve to qualitatively compare the different calibration methods in regards to their precision and the challenges in their application.

TABLE OF CONTENTS

LIST OF FIGURES

LIST OF TABLES

Dedicated to the memory of my Father, Elias Helou (1956-2012)

Chapter 1

INTRODUCTION

1.1. Objectives and Motivation

The constant demand for faster, smaller and more efficient electronic devices has been driving the development in the microelectronic industry. Advancement in the fabrication process has lead to a miniaturization in the size of transistors leading to a trend in enhanced performance and boost in productivity, known as Moore's law. Smaller features in the size of transistors also meant that the switching time is shortened and the required power to create the conducting channel is reduced. However, the compact dimensions needed for fast and efficient transistors, and the increase in the number of devices per wafer, as well as the use of electrically and thermally insulating material in the device structure, all result in higher operating temperatures and localized hot spots. At elevated temperatures, mechanical and thermophysical properties change drastically and deviate from design tolerances thus critically affecting the performance and energy efficiency of a device, potentially causing unpredictable electronic behavior and eventually leading to a shorter lifetime and premature failure [14].

The thermal challenges accompanying high power microdevices led to the need for a measurement technique to thermally diagnose and analyze device failure. Temperature mapping was required to identify hot spots, assess thermal performance of structure designs and characterize the heat dissipation effectiveness of thin film materials used in the fabrication process. For that purpose several thermal imaging techniques were developed with different physics and specifications to provide fast and reliable surface temperature maps with good accuracy and a spatial resolution that scales down to the feature sizes of the microelectronic device.

1.2. Thermal Microscopy Techniques

The most commonly used thermal imaging technique is the infrared thermometry (IR). Pyrometers also known as radiation thermometers measure the amount of radiation emitted from a body and infer the temperature by Planck's law [6]. This method acquires non-contact temperature maps at the macro scale, but fail to detect spatial resolutions below a few microns due to the diffraction limit of infrared radiation. Samples covered with gold or other shiny metallic surfaces have low emissivity and are inefficient at emitting infrared radiation. Testing with IR thermometers requires a surface with high emissivity; thus samples are often coated with a thin coating "target" of black paint, which also would alter the thermal properties and response of the sample under test.

To achieve temperature measurements at the microscale, thermal engineers resorted to micro-thermocouples, either embedded in the structure of the device or mounted on a tip that engages contact at the surface of the device. These techniques utilize contact methods to obtain single point measurements. Mapping a surface for a temperature distribution requires an additional translation stage for moving the tip across the area. Although the temperature detected is accurate to 0.01 K, the spatial resolution is limited to the size of the thermocouple tip (25-50 microns) [6].

Scanning thermal microscopy (SThM) is another technique that can improve on the spatial resolution by using nanometer size thermocouple fabricated at the tip of an AFM probe. The method is highly accurate but proves to be expensive and not commercially available, time consuming and erroneous for light emitting samples that radiate to the probes and alter their temperature.

To obtain complete thermal images of the field of interest, non contact methods are preferred over contact methods since the temperature map is obtained remotely without interfering with the sample and introducing heat conduction paths that affect the temperature. Moreover, non contact methods provide instant thermal images that do not require translational stages and the accompanying long acquisition times. The thermoreflectance technique has been in development as a non invasive, non contact and non destructive method to ob-

tain thermal images. However, the accuracy and reliability has been dependent on the light detector precision and the ability to detect the small changes in reflectivity of the surface due to a temperature change.

Thermoreflectance resolution can reach 0.3 to 0.5 microns and a 0.01 K [6]. Thermoreflectance microscopy started with single point measurements and later a micro-positioning stage was used for an extensive scan over the whole area under test. With the improvements in charge coupled device (CCD) technology, cameras were used in detecting the intensity changes with relatively low noise levels that would not mask the thermal reflectivity effects.

The technique is used to measure surface temperature and was also utilized in pump and probe property measurements [3,5] where the temperature is monitored while a laser excites the surface. The energy absorption and the temperature decay through the microelectronic stack is monitored and analyzed to infer the stack's thermal properties.

1.3. Thermoreflectance Effect

Thermoreflectance imaging techniques operate on the basis that the reflectance of a surface is dependent on temperature. Reflectance of a surface is the ratio of the amount of incident light that is reflected back. By acquiring the changes in the intensity of reflected light, the measurement setup can infer the change in temperature. The relation between the reflected light intensity and the temperature has a dominant first order dependence shown in Eq. 1.1.

$$R(T) = R(T_0) + \frac{dR}{dT}(T - T_0) + \frac{1}{2}\frac{d^2R}{dT^2}(T - T_0)^2 + ... \tag{1.1}$$

$$R(T) = R(T_0)(1 + \kappa(T - T_0)) \tag{1.2}$$

The linear parameter $\kappa = \frac{1}{R}\frac{dR}{dT}$ is often referred to as the thermoreflectance coefficient also represented in the literature as C_{TR}.

The ratio of reflected light and thus the thermoreflectance coefficient are dependent on the surface material composition, roughness, the light's optical path and wavelength. For that reason, to obtain a temperature reading from a reflection intensity measurement, the coefficient of thermoreflectance has to be first acquired through a calibration run according to Eq. 1.3 which can be done using one of the methods presented in Section 2.2.

$$C_{TR} = \frac{\Delta R/R}{\Delta T} \tag{1.3}$$

The reflectance of a surface has been demonstrated to be weakly sensitive to temperature changes where the coefficient of thermoreflectance lies in the range of 10^{-5} to $10^{-4}K^{-1}$ which proves the detection of such changes to be challenging [2]. To be able to acquire a sufficient signal to noise ratio, the surface is required to be reflective, and to be sufficiently thermally reflective. For most metallic surfaces used in microelectronic fabrication like Gold and Aluminum, the surface is reflective and provides a sufficient amount of reflected light. However, for a surface te be thermally reflective, it must exhibit reflectance changes with temperature under some specific wavelength of illumination. Different photon energies interact differently with the surface and thus the incident light wavelength that results in the maximum reflectance change signal output needs to be determined. This is done by scanning through different wavelengths of light while measuring the reflectance change as presented in Section 4.1.

1.4. Outline

This work will investigate the linear assumption of the reflectance-temperature relation used in calibration of thermoreflectance instruments for temperatures between 20°C and 100°C and studies how this assumption can affect the accuracy of temperature measurements. In the next section, a literature review will present the theory behind the temperature reflectance relation and the experimental processes and the assumptions used in the

field for calibration. In the study presented by this work, several calibration techniques will be assessed for their accuracy and precision and a single-point phase-locked measurement procedure will be described in Section 4.2 and used for high precision measurements of the thermo-reflectance coefficient. The results will be validated in Section 4.3 and 4.4 by a thermo-electrically (TE) controlled stage heating and a self-heating CCD calibration method.

Chapter 2

LITERATURE REVIEW

The thermoreflectance technique is mainly used as a measurement approach for the steady [12] and transient surface temperature response [3] of activated micro-devices. The experimentally obtained measurements also served in many studies as inputs and result validation data for computational method [15, 16]. By combining experimental and thermal models, input parameters can be iterated to determine thermo-physical properties such as the conductivities and interface resistances of multi-layered structure of complex micro-devices.

2.1. Theory of Reflectance Temperature Dependence

Reflectance of light from a surface is an interaction between the electromagnetic incident wave and the energetic structure of the material. The electromagnetic wave can be either absorbed, transmitted or reflected, with ratios depending on the optical properties of the surface, determined by the energy of the lattice, and the energy of the incident photons. Reflectance from a surface, by Fresnel equations, is calculated in terms of the complex refractive index $N = n + ik$.

$$R = \left|\frac{1-N}{1+N}\right| = \frac{(1-n)^2+k^2}{(1+n)^2+k^2} \tag{2.1}$$

The reflectance change appearing in the expression of the thermoreflectance coefficient in Eq. 1.3 can be expressed by differentiating Eq. 2.1.

$$\frac{\Delta R}{R} = \left(\frac{4N}{N^2-1}\right)\frac{\Delta N}{N} \tag{2.2}$$

The refractive indexes can be determined from the complex dielectric function $\epsilon = \epsilon_1 + i\epsilon_2$

$$n = \left(\frac{(\epsilon_1^2 + \epsilon_2^2)^2 + \epsilon_1^2}{2} \right)^2 \tag{2.3a}$$

$$k = \left(\frac{(\epsilon_1^2 + \epsilon_2^2)^2 - \epsilon_1^2}{2} \right)^2 \tag{2.3b}$$

Consequently, the reflectance of a surface can be expressed in terms of the change in the real and complex part of the dielectric function by combining Eqs. 2.1 and 2.3 and differentiating with respect to ϵ_1 and ϵ_2 [20].

$$\frac{\Delta R}{R} = \frac{1}{R}\frac{\partial R}{\partial \epsilon_1}\Delta\epsilon_1 + \frac{1}{R}\frac{\partial R}{\partial \epsilon_2}\Delta\epsilon_2 \tag{2.4}$$

The partial derivatives expressed in terms of ϵ_1, ϵ_2, and $\epsilon = \sqrt{\epsilon_1^2 + \epsilon_2^2}$ are shown in Eq. 2.5

$$\frac{1}{R}\frac{\partial R}{\partial \epsilon_1} = \frac{\sqrt{2(\epsilon_1 + \epsilon)}}{\epsilon((\epsilon_1 - 1)^2 + \epsilon_2^2)}(2\epsilon_1 - \epsilon - 1) \tag{2.5a}$$

$$\frac{1}{R}\frac{\partial R}{\partial \epsilon_2} = \frac{\sqrt{2}}{\epsilon\sqrt{\epsilon_1 + \epsilon}((\epsilon_1 - 1)^2 + \epsilon_2^2)}(2\epsilon_1 + \epsilon - 1) \tag{2.5b}$$

The above relation has allowed the complex dielectric function $\epsilon = \epsilon_1 + i\epsilon_2$ to be calculated from modulated reflectance measurements in spectroscopic ellipsometry. The dielectric function determines the energy structure of metals and semiconductors. The optical reflectance is dependent on the structure of the energy band and on the process involved in its interaction with incident electromagnetic waves. For intraband processes, the free carriers are the major contributors in defining the interaction, which occur mostly in metals and conductors. For interband processes, the optical properties are defined by electrons at low energy levels absorbing the incident radiation and transitioning to higher energy levels, which is the case for semiconductors [1].

Since the 1960's, temperature-modulated reflectance was used to measure the band structure of gold. One reflectance measurement is not sufficient to obtain the real and complex

part of ϵ, thus, a scan has to be performed for either the incident angle or the photon energy spectrum. To obtain a comprehensive understanding of energy interactions with the structures, a wavelength scan was more convenient with photon energies ranging between 2 ev (λ=620 nm) and 10 eV (λ=124 nm).

In addition, the temperature variation of C_{TR} was investigated from the optical point of view, but the studies did not utilize continuous temperature scans. Most recently by Reddy et. al. the dielectric function and the refractive indexes were measured at distant temperature levels (23°C, 100°C, 200°C, 300°C) [17]. Also optical studies are more concerned with the energy band structure and the spectral variation of the dielectric function. Temperature variations cause shifts and warps in the band structure.

Temperature change can affect the complex dielectric function and the energy structure of solids in several ways [18]:

1. Volumetric expansion causes the electron density to change and the Fermi level to shift
2. Shear stress resulting from sample constraint in the substrate can also cause shifts and warps in energy bands
3. Broadening distributions around the Fermi level
4. Phonon population increase causing less electron relaxation times and shifts and warps due to electron-phonon interaction
5. Temperature changes cause small increase in the Fermi level
6. Flowing electric current in Joule heating displaces the energy distribution function

In a simplified approach the change of the dielectric function can be caused by a change in temperature and is related in solid state physics by a shift in the band gap energy E_g and the broadening parameter Γ in the case of semiconductors and to the DC electrical conductivity in the case of metals. However at large temperature changes the effects can cause nonlinear variation in the C_{TR} coefficient and affect the accuracy of thermoreflectance microscopy techniques [1]. For thermoreflectance experimental studies, and unlike theoretical

approaches, the overall combined effect of temperature on the reflectance is acquired by calibration at a given light wavelength (phonon energy), without the need for full photon energy spectrum analysis.

2.2. Linear Calibration Methods

The coefficient C_{TR} in principle is obtained by measuring the reflectance at different temperature levels. This calibration process is required to obtain the relation between the temperature rise and the reflectance change to be able to activate the device and translate reflectance into temperature maps. In most applications of the metrology tool, the reflectance coefficient is assumed to be constant for several reasons.

The linear assumption stems from the fact that the technology started with low precision CCD imaging and without phase-locking. Thus the weak second-order effects cannot be recognized as seen in the results obtained by Tessier *et. al* in Fig. 2.1 and other independent studies [9, 13, 23]. Thus, for practical reasons, the relation is assumed linear with a constant first-order term C_{TR} while the higher-order terms are neglected.

To test the accuracy of the optical measurements, Tessier *et. al* validated the results with finite element simulations. A linear calibration profile was used to calculate temperature rises that exceeded 140 K. A small deviation from the numerical results was observed at high temperatures which could be associated with either C_{TR} change with temperature or thermophysical changes that were not considered in the computational method [23].

The linear assumption of the reflectance-temperature relation turned out to be very practical since it provides a fast calibration run without the need for measurements at the full temperature range, thus saving time from the slow first-order heating of the system.

2.2.1. Thermo-electric Differential Calibration

This straightforward calibration method heats the sample using thermo-electrical (TE) heating stage to two distinct temperatures at which the reflectance distribution at the surface is measured. By calculating the change in the reflectance, the coefficient can be calculated

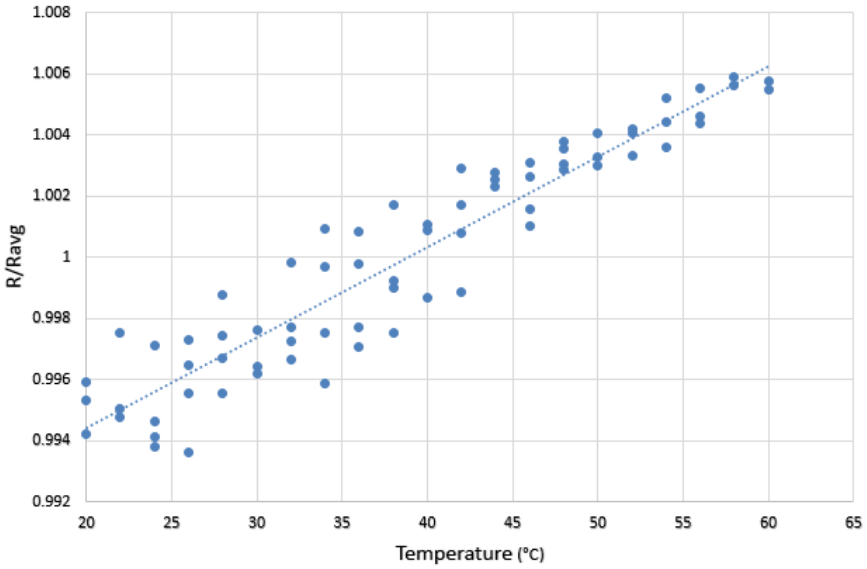

Figure 2.1. Reflectance variation with temperature obtained with CCD Thermoreflectance. Source: Tessier *et al.* [23]

at each location on the sample's surface. The method has some drawbacks where the entire heating causes thermal expansion and shifting of the field of view under high magnification that requires realignment and refocusing. In addition, at elevated temperatures convective effects start affecting the optical path of the system.

The changes in reflectance are extremely small and can be as small as a 0.1% change per degree. Another reason for the low precision of TE calibration measurements is the absence of phase locking to the heating phenomena. Phase locking to the heating is not suitable since the lock-in detector would drift at the low frequencies of the heating and cooling cycle.

2.2.2. Phase-Locked Measurements

Other studies investigating the coefficient of thermoreflectance and its dependence on temperature conducted more precise phase-locked calibrations that provided more robust measurements that filtered thermal drift or background irradiation. The locking mechanism was performed by increasing the frequency of heating cycles or by using a modulated light source.

In a study conducted by Schlag *et al.* [19], the C_{TR} was assumed constant for temperatures below 100 K and was calculated for different silicon, gold and aluminum samples. Relation was dominated by the first-order term for the wavelengths used (639 and 670 nm) and the higher order terms were insignificant. The choice of wavelength was not justified for better thermal response but different LED's were compared for their electric current intensity linear curve for modulation capabilities and their relative stability. The second-order effects can also be dependent on wavelength and become more pronounced for different photon energies.

Also thermal drift problems were not corrected and only minimized by choosing a heater with minimal drift. The sample may have moved out of focus which reduces the precision of the instrument, and this would limit the setup to take spot measurements of bare metallic samples. This proves that the system is not viable to calibrate a complex device with different surface material and structures. To use the averaged C_{TR} values obtained through measuring different samples would lead to an accuracy error shown to be in excess of 20°C [19].

Favaloro *et al.* [8] used self-heating resistor activated with the 3ω method to calculate the temperature rise and a CCD camera locked in to the heating cycle to calculate the reflectance change. The C_{TR} for different metals were calculated at temperatures reaching 500 K and showed a variation of around 0.3×10^{-4} per 100 K temperature for gold. The method is insensitive to thermal expansions since the heating is localized and the CCD detection can obtain an image of the whole surface structure. Some drawbacks are that testing under temperatures reaching 500 K required that the sample be placed in a vacuumed optical thermostat and that the optical beam be projected through a transparent sapphire window. This introduced a new medium in the path of the light beam and resulted in a shifting effect on the C_{TR} [8]. The additional transparent layer can create multiple reflections and interference effects that can weaken the reflected signal. Moreover, calibration setup should match the activation setup to ensure that the thermal reflectance coefficient reflects the same conditions. A vacuum chamber may therefore introduce further complexities to reach the device optically and activate it electrically.

Chapter 3

EXPERIMENTAL SETUP AND METHODOLOGY

3.1. Phase-Locked Differential Measurement

The detection of second-order effects of C_{TR} requires a very high precision calibration setup. The setup used for this study utilized several techniques to ensure the noise level is kept at its minimum and that the signal is enhanced. The thermoreflectance coefficient (C_{TR}) was measured using a single-point measurement setup depicted in Fig.3.1. The photodetector has less noise than a CCD camera, along with phase-locking, and acquiring a balanced differential measurement provides high precision and more accurate readings.

The illumination used is monochromatic light supplied by a Horiba Monochromator. The modulation is done by a speed controlled light chopper set at 200 Hz which is distinct from the ambient illumination and its harmonics. The light beam is then passed through a polarizer and a collimator to provide a straight polarized beam of light. A beam sampler then diverts a portion of the light to a photo-detector (PD1) that monitors fluctuations in the source for correction. The remaining beam is directed through an optical setup consisting of a polarizing beam splitter cube and quarter wave retardation plate and finally focused through an objective lens onto the sample at normal incidence. The light reflects back through the same path towards the quarter wave retardation plate and through the polarizing cube beam splitter to the second light sensitive photodetector (PD2).

The optical components are chosen as to optimize the light path and to ensure the maximum amount of irradiation reaches the sample and reflects back to the photodiode. The reflected light intensity from a black porous sponge is measured at the beginning of each run to quantify and remove the amount of light reflecting internally in the system. This would ensure that any detected light at PD2 is entirely reflected from the sample and

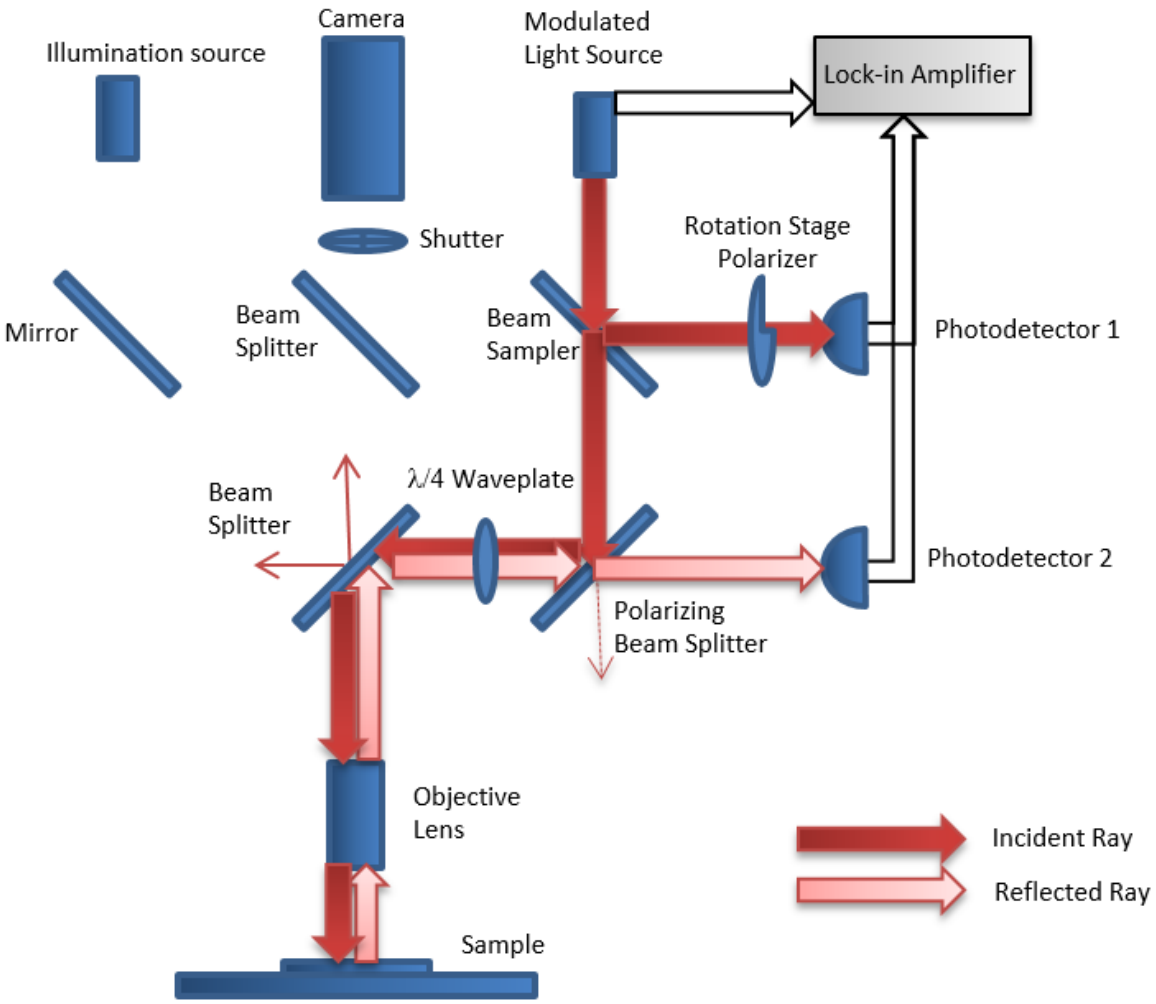

Figure 3.1. Phase-Locked Differential PD Setup in measurement mode

not from stray light reflections from the optical setup.

The sample consists of a gold layer of 100 nm thickness deposited on a Silicon wafer with an intermediate 10 nm thick Chromium glue layer. The sample is placed and vacuum held on a thermal chuck built by TMX Scientific® that can control the temperature within 0.1 K. A 20× objective lens is used to focus the beam of light onto the sample with a spot size of less than 0.5 mm. The setup has a CCD camera and a white light illumination source used to position the sample surface as shown in Fig.3.2. This would also allow to measure C_{TR} of different materials on the surface of a device by moving the XYZ positioning controls beneath the stage without any handling of the sample. The white light is used for illuminating the source for positioning while the focusing is done under the wavelength of light used for testing.

At the source sampling end, the light intensity reaching PD1 is attenuated using a polarizing film mounted on a computer controlled rotation stage until the differential measurement is less than 1% of the reflected light intensity at PD2. The attenuated intensity acquired by the reference PD1 is thus set equal to the initial reflectance intensity at the base temperature T_1. The balancing of the photodetectors at the initial calibration temperature would result in a more precise measurement since the temperature induced differential reflectance signal would occupy the full range of the digitizer.

The balanced photodetector signals are then pre-amplified and acquired by an SR 830 DSP Lock-In Amplifier which is phase-locked to the frequency of the light source chopper. This will filter out all other ambient and interfering light that is not modulated at the prescribed frequency. Any change in the lock-in differential measurement is the result of a change in the intensity of reflected light since the sampled light source (PD1) is invariant with the temperature change. In this manner, the coefficient of thermoreflectance can be calculated as follows:

$$C_{TR} = \frac{\Delta R}{R}\frac{1}{\Delta T} = \frac{R_h - R_c}{R_c}\frac{1}{\Delta T} \tag{3.1}$$

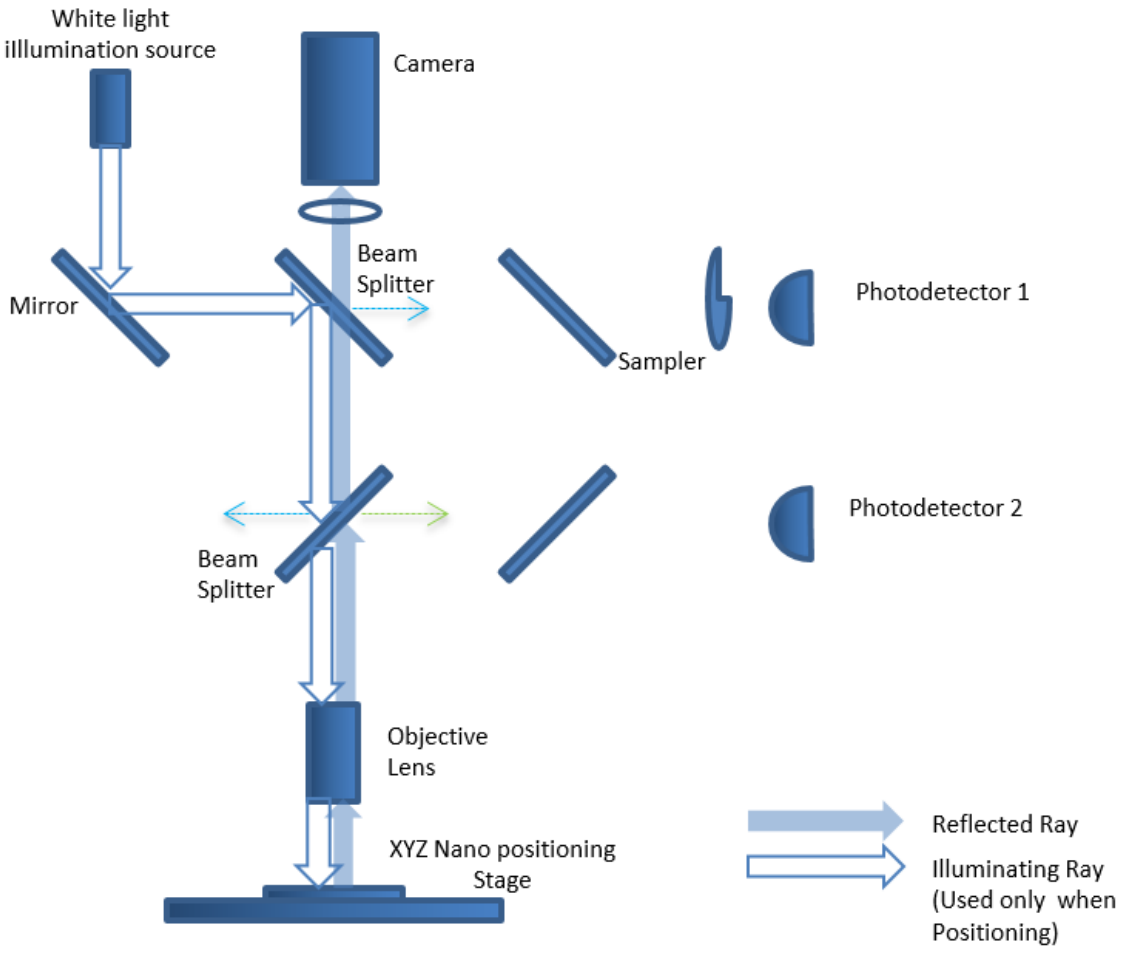

Figure 3.2. Phase-Locked Differential PD Setup in alignment mode

The subscripts c and h will indicate the cold and hot temperatures respectively at which the reflected intensity is measured while 1 and 2 will represent the respective photodetector.

The voltage potential E of a PD is proportional to the intensity of light R reaching its light sensitive area. Thus the ratio of intensities can be represented by a ratio of the photodetectors' pre-amplified electric potential E.

$$\frac{\Delta R}{R} = \frac{E_{2h} - E_{2c}}{E_{2c}} \tag{3.2}$$

Using a differential measurement, the source sampling PD1 voltage is subtracted from the intensity of reflected light read at PD2 and balanced to zero at the low calibration temperature.

$$\frac{\Delta R}{R} = \frac{(E_{2h} - E_1) - (E_{2c} - E_1)}{E_{2c}} = \frac{dE_h - dE_c}{E_{1c}} = \frac{dE_h}{E_1} \tag{3.3}$$

The difference symbol Δ represents the change between the two reflected intensity measurements at different temperatures while the symbol d represents the differential nature of the measurement $E_2 - E_1$ between PD2 and PD1.

The value of $\Delta(dE) = dE_h - dE_c = dE_h$ is acquired at the high temperature measurement since dE_c is balanced to zero. The reflected intensity of light E_{2c} is obtained from the initial balancing of the two photo-detectors and can be measured at T_c from either PD1 or PD2. To obtain a temperature invariant reading, $E = E_1 = E_2(T_c)$ is measured from PD1. The coefficient is finally calculated using Eq. 3.4 and averaged over 10 heating and cooling cycles.

$$C_{TR}(\lambda) = \frac{dE_h}{E_1}\frac{1}{\Delta T} \tag{3.4}$$

By definition, the C_{TR} coefficient is prescribed as a differential value $C_{TR} = (\partial R/\partial T)/R$. In practice however, the C_{TR} is measured as a difference between two distinct temperatures. The C_{TR} value in this article will be reported at a central temperature while also prescribing the temperature change imposed to acquire the reflectivity signal. Therefore a value for $C_{TR}(T, \Delta T)$ would represent a calibration between $T - \Delta T/2$ and $T + \Delta T/2$.

3.2. CCD Measurement Setup

In order to acquire a surface temperature map instead of a single-point measurement, the thermoreflectance technique has been extended to acquire a thermal map by using a photodiode array or a CCD camera instead of a single PD. A single-point scanning method was initially used with a translation stage to acquire the image point by point, but the method proved to be time consuming [7]. The CCD camera has a lower sensitivity than the photodiode array but can acquire a larger image with more pixels and better resolution. To obtain a thermal image, the reflected intensity is combined with the C_{TR} coefficient map at every pixel (i,j) within the field of view using the definition of C_{TR} from Eq. 1.3.

$$\Delta T(i,j) = \frac{\Delta R(i,j)}{R(i,j)} * \frac{1}{C_{TR}(i,j)} \tag{3.5}$$

By fixing the temperatures at two distinct levels and measuring the surface reflectivity, the CCD system can be used to calculate the C_{TR} surface map using Eq. 3.2. Several challenges arise when measuring local reflected intensity variations at the nano-scale. Heating a sample leads to thermal expansion of the device, and with great magnifications of features lying in the sub-micron scale, the captured images at the high and low calibration temperature undergo a spatial displacement. To ensure that the pixel-by-pixel calculation for C_{TR} involves the same physical location on the surface of the device [4], an XYZ piezoelectric translation stage is required for realigning the image to its initial location before every set of frames is acquired. The Z-stage ensures optimal focus and that the z position is the same for all frames.

In this study, the TMX Scientific T°imager® thermal imaging system, depicted schematically in Fig. 3.3 was used for validating the C_{TR} measurements. For simplicity, the device activation setup is not presented in the schematic, and only the optical system, the thermal chuck and the light source used for calibration are shown. A photodetector monitors the intensity of the source illumination to correct for any fluctuations that might affect the

reflected intensity signal.

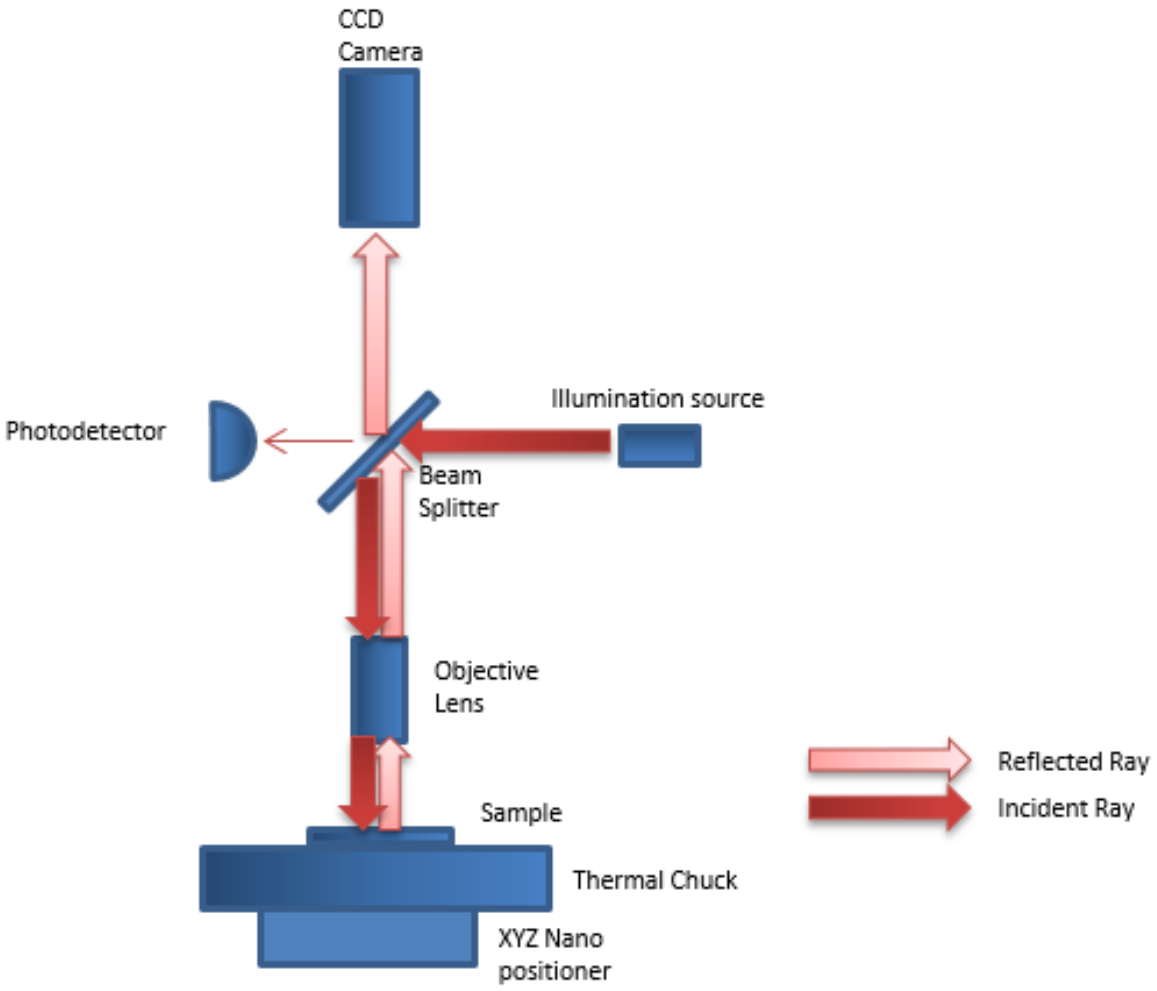

Figure 3.3. CCD setup used in Calibration mode

3.3. In-Situ Micro-resistor Heating Setup

An additional in-situ technique was used to measure the thermoreflectance coefficient and validate the results. In this method, the temperature rise of the sample is generated by self heating of a microresistor by electrical activation at a certain power level. By heating the localized metallic strip instead of the whole sample and the thermal base, the effects of

convection plumes that interfere with the optics of the system are reduced to a minimum. Moreover, by heating a localized region of the sample and not the whole thermoelectric stage, the thermal expansion effects are avoided and no XYZ nano-positioning stage for realignment and refocusing is needed. This calibration technique is the most faithful representation of the actual activation of a device since high temperature conditions will be localized to small hot spots and the convective plumes would be kept to a minimum. In addition, the localized heating would not require the placement of the device in vacuum chambers which increase further the complexity of the setup and the accessibility to the device optically and electrically.

The sample resistor for this method is used as the heating source and the temperature sensor where the amount of power dictates the rise in the resistor's temperature. The microresistors used are deposited gold strips 5, 10, 20 and 30 μm wide with fabricated features as depicted in Fig. 3.4. The four pads are used for microprobes connections that will activate the resistors.

The resistance is measured using the four-probe method contact pads in which the resistance is monitored and its change with respect to the mean temperature rise of the metallic strip is obtained. The four-probe method uses two sets of contacts, the forcing and the sensing probes as labeled in Fig. 3.4. The forcing terminals induce a constant current through the resistance while the two sensing probes measure the voltage across the resistor. By

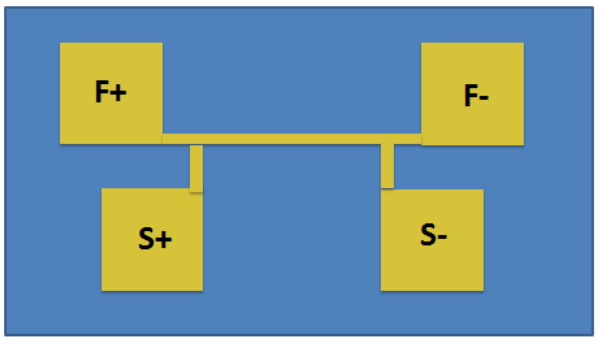

Figure 3.4. Micro-resistor structure showing the pads for four-probe activation

comparing the voltage and current, an accurate reading for low resistances can be inferred without including the resistances of the connections and the contact resistances [21].

The four-probe measurements are performed using an HP 4142B Modular DC Source Monitor Unit (SMU) that can measure high ranges (1000V and 10A) and with high precision (4 μV and 20 fA). The DC SMU is highly accurate with errors as low as 0.05% for voltage readings and 0.2% for current intensity readings. The DC SMU is also used for applying and monitoring the DC power for the Joule heating in the activation stage.

The temperature coefficient of resistance α is obtained first by measuring the electrical resistance at different base temperatures set by the thermoelectric (TE) element in the base. The four-probe method is used with a low applied power to minimize self-heating. The linear coefficient is calculated as the relative change in resistance per degree temperature change as shown in Eq. 3.6,

$$\frac{\Delta\Omega}{\Omega} = \alpha\Delta T \tag{3.6}$$

The probes are lifted before each temperature change to avoid any damage to the tungsten needles from thermal expansion. After the system reaches a stable temperature the needles are lowered and contact with the pads is reestablished.

To obtain the average temperature rise for an applied electrical power, the activation resistance change must be related to the applied power as well. The linear power-temperature and temperature-resistance relations yield a linear power-temperature relation that is presented by Eq. 3.7,

$$\frac{\Delta\Omega}{\Omega} = \beta P \tag{3.7}$$

The sample is vacuum held at the thermal chuck and the base temperature is set to 20°C to within ±0.1°C. After ensuring good contact with the probes, different voltage levels are applied and the current is accurately monitored by the use of the four-probe method. The applied power would cause the resistor self-heat and its electrical resistance to change.

Combining Eqs. 3.6 and 3.7 gives the average temperature rise in the resistor for a certain applied power level as shown in Eq. 3.8.

$$\Delta T = \frac{\beta}{\alpha} P \tag{3.8}$$

The methodology for calculating C_{TR} begins with determining the linear coefficients α and β as described above. Then, the required power level is applied for each desired temperature level, and the CCD camera acquires a set of 200 frames to obtain the averaged intensity of reflected light over a region on the gold microresistor. Finally, a value of C_{TR} between the two temperatures T_1 and T_2 is calculated, using the modified Eq. 3.9.

$$C_{TR} = \frac{\Delta \overline{R_{avg}}}{\overline{R_{avg}}} \left(\frac{\beta}{\alpha} \Delta P \right)^{-1} \tag{3.9}$$

The avg subscript refers to the spatial average intensity over a surface area on the gold micro-resistor. The bar refers to a statistical average over the 200 frames obtained from the CCD camera and corrected with the PD voltage reading. Finally, the Δ notation refers to the difference between two activation temperatures of the resistor. For simpler notations, the variable R will be used in the equations that follow to represent the corrected and averaged reflection intensity.

Each image obtained by the CCD camera is a 498×498 array of pixels where each pixel is digitized at 16 bits and therefore falls in the range of 65,536 shades of grey. The reflected light intensity at the low temperature level was set to around 40,000 by modifying the camera exposure time to ensure the overexposed regions would not saturate the camera.

The assumption taken in this method is that the resistor is at an average temperature. The measurements are taken at a location away from the boundaries to avoid the effects of conduction into the pads, and to ensure that the temperature is uniform along the length of the resistor for a constant heat source. Since the calibration of the linear coefficients α and β also compares the applied power effect to an average temperature increase, the assumption is valid for reporting the temperature as a mean value.

Chapter 4

RESULTS AND DISCUSSIONS

4.1. Wavelength Scan

Before the C_{TR} temperature calibration, the optimal wavelength for testing needs to be determined. This would ensure that the material is sufficiently thermally reflective, i.e. the reflectivity change due to temperature is large enough to obtain a good signal to noise ratio. For that reason, a scan over the visible light spectrum was performed while heating the sample using the thermal chuck and monitoring the reflectivity response. A monochromator provided the variable wavelength illumination used between 400 nm and 650 nm with a bandwidth of 2.5 nm and 5 nm . The gold covered sample was heated from 20°C to 40°C at every wavelength using the setup mentioned in Sections 3.1 and 3.2. C_{TR} was calculated using the linear assumption by Eq. 1.3. Figure 4.1 shows the results of the scan that match the reported values by Burzo *et al.* [3] for gold and validates the calibration setup.

A small deviation from the reference values is seen at the low end of the spectrum because of loss of light intensity from the monochromator resulting in a lower signal to noise ratio. The broader bandwidth also resulted in a reduced peaks for the measurements caused by an integration effect.

The peak response signals occur at wavelengths of $\lambda = 480nm$ where $C_{TR} = 4 \times 10^{-4} K^{-1}$ and at $\lambda = 520nm$ where $C_{TR} = -3 \times 10^{-4} K^{-1}$. The wavelength for the calibration is thus chosen as 480 nm.

4.2. Phase-Locked Differential Measurement

The first method used a differential photo-detector reading which is locked in at the frequency of the illumination source. The C_{TR} coefficient was calculated at temperatures

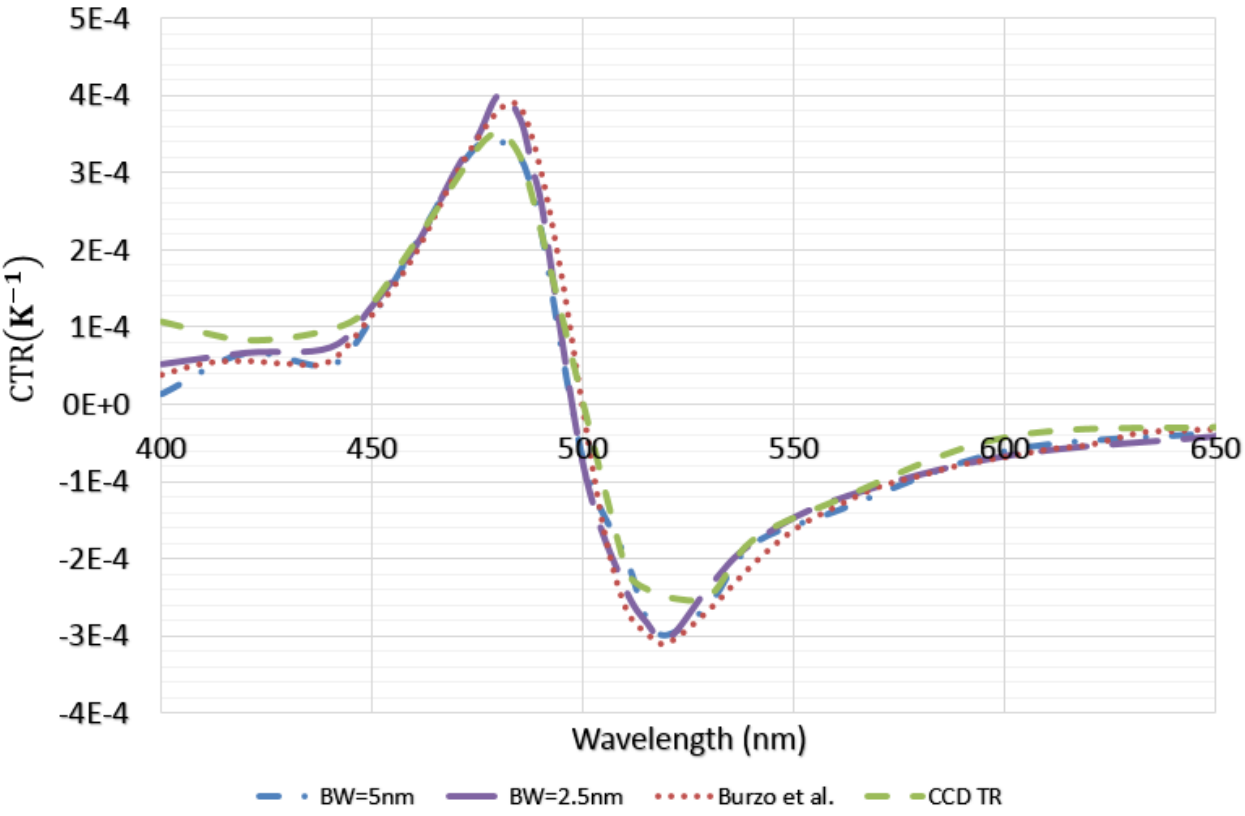

Figure 4.1. Thermal Reflectance Coefficient Scan of Gold under different illuminations wavelengths

ranging between 25°C to 100°C. The calibration was performed with sample temperature rise of 4, 10, and 20°C as shown in Fig. 4.2 to compare the results and comment on the sensitivity of the measurement setup.

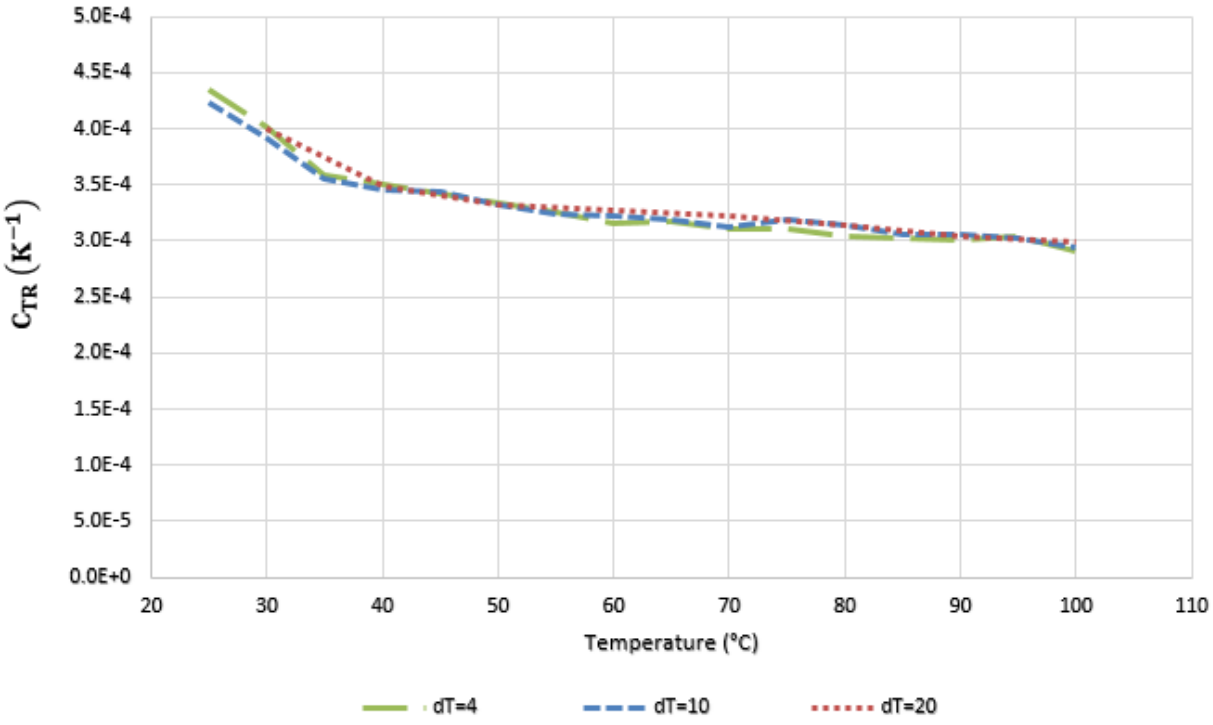

Figure 4.2. Coefficient of Thermoreflectance Variation with Temperature

When elevated to a high temperature the heated chuck caused natural convection effects and entrained air into plumes that rose from the chuck and altered the optical path. The mixing of hot and cold air plumes created optical effect that could be seen as fluctuating reflected light intensity when observed through the CCD camera. For this reason, a conical nozzle was fitted to the objective lens and its tip lowered to close proximity to the sample to isolate the measurement location. An observation with the CCD camera showed that the cone removed the fluctuations in the reflected intensity of light. This approach was used instead of a vacuum chamber because of the reasons stated in Section 2.2.2 and since the convection currents are not that drastic for a maximum temperature of 100°C.

The results plotted in Fig.4.2 show a decrease in the C_{TR} value from $4 \times 10^{-4} K^{-1}$ at 25°C to around $3 \times 10^{-4} K^{-1}$ at 100°C, a decrease of 25%. This trend is observed for the different ΔT values at elevated temperatures. The system proved perfectly capable of detecting down to a reflectance change signal of $\Delta R/R = 1.5 \times 10^{-3}$ (0.15%) for $dT = 4$°C whereas the CCD thermal imaging requires a temperature rise of at least 10°C to obtain a adequate signal to noise ratio. The light chopping and the lock-in detection, along with the zeroing differential measurement, allowed the system to detect minute changes that would otherwise be undetectable if the noise had not been filtered out and the signal enhanced.

4.2.1. Accuracy Assessment

In this section, a comparison is done for temperature rises from a reflectance measurement assuming constant C_{TR} versus a more accurate calculation using the C_{TR} distribution obtained in the previous Section 4.2.

Knowing that the coefficient was calculated using a differential measurement at each temperature level, the absolute reflectance change from room temperature was reconstructed using a numerical integration of the C_{TR} coefficient using Eq. 4.1.

$$\frac{\Delta R}{R} = \int_0^T C_{TR}(T) dT \tag{4.1}$$

Since most devices are activated at room temperatures, the initial slope chosen from calibration determines the accuracy of the measurements at high temperatures. As the results show, the coefficient is not constant being around ambient conditions at $4 \times 10^{-4} K^{-1}$ but gradually decreases by up to 25% at 100°C. Choosing the initial value would overestimate the slope and underestimate the temperature rise.

The curve presented in Fig.4.3 shows that the reflectance variation is dominated by a linear component but also exhibit second-order variation. The reflectance change was compared to an extrapolated linear relation using coefficients for a 20-40°C rise and 50-70°C calibration. A second-order fit follows the relation very closely and could be used to determine the temperature rise for any activation level. The result shows that even for a

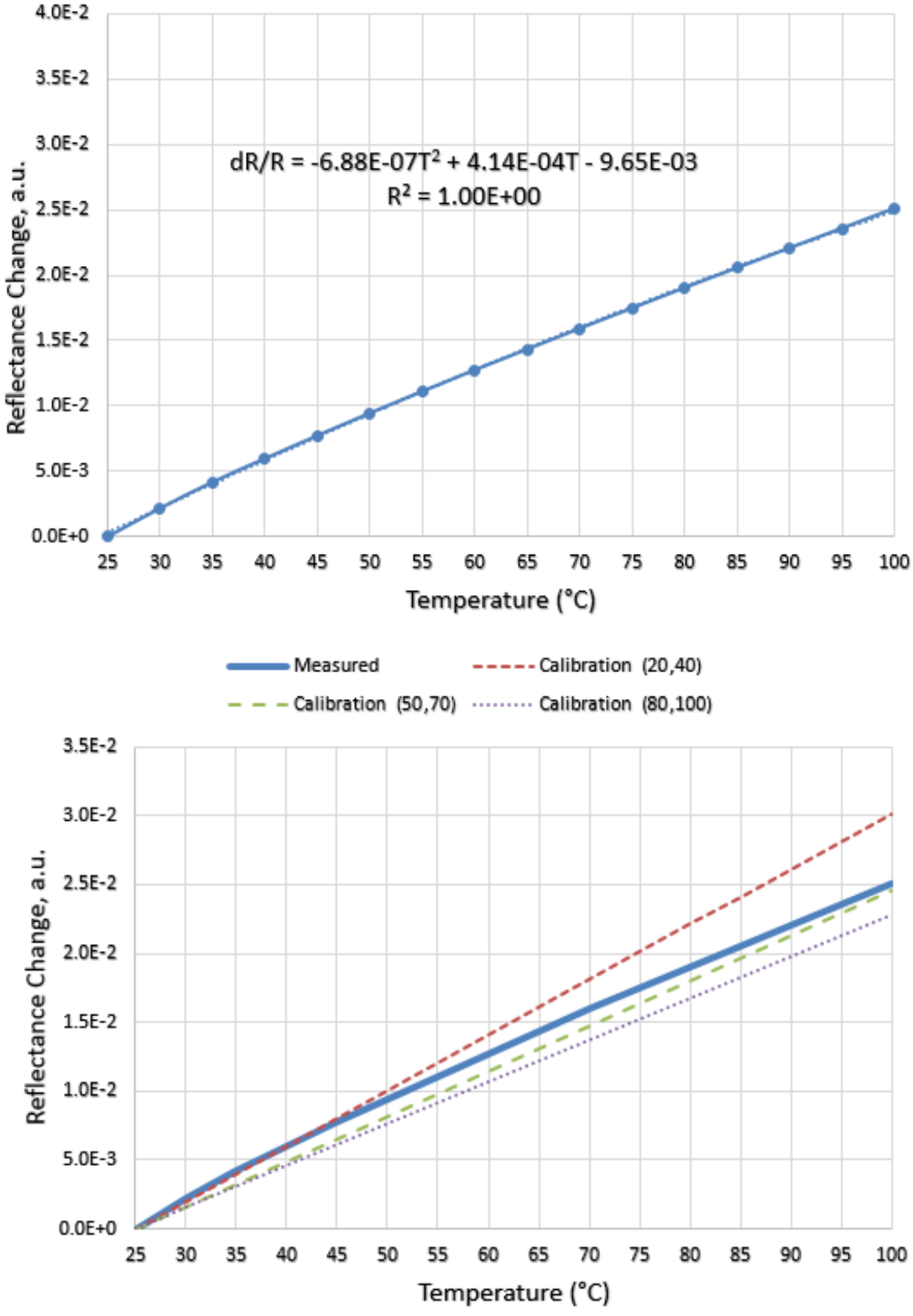

Figure 4.3. Measured Reflectance Temperature Variation compared to Linear Approximations

small second-order effect, the choice of calibration and the range of temperature changes can lead to an accuracy error in excess of 10°C. If a linear calibration is done, the constant C_{TR} should be chosen carefully to minimize the accuracy error. It is advised to calibrate from ambient conditions up to an approximated maximum temperature rise to limit the error.

The reflectance-temperature curve in Fig. 4.3 also shows that the nonlinear effects are mostly prevalent at low temperatures with the curve becoming more linear above 60°C. More accurate linear calibrations can be done starting from an initially heated sample but that would require to also heat the sample to an elevated initial temperature before activating. Another suggestion can be to perform a two point calibration while calibrating up to a temperature in the vicinity of the max operation temperature which will reduce errors at the high ranges but the accuracy at low temperatures will worsen. To further improve on the accuracy, the linear approximation can be replaced by a higher-order relation obtained by a three temperatures calibration and a second order fit.

4.3. CCD Measurement Results

The calibration using the TMX Scientific T°Imager® where 200 frames were obtained at two temperature levels for three heating and cooling cycles. The frames were then averaged and corrected for source fluctuations. A differential intensity calculation along with the known temperature difference gives C_{TR} at each location. A spatial average is taken on the gold sample surface at temperatures between 20°C and 100°C. The averaging was done for the 3 heating and cooling cycles which gives five C_{TR} values repeated for two to three trials. The results are shown in Fig. 4.4.

The trend observed with the CCD imaging system is that the C_{TR} coefficient drops slowly from a value of around $3.7\times10^{-4}K^{-1}$ at 25°C to below $3\times10^{-4}K^{-1}$ at temperatures in excess of 60°C which validates the initial observation with the phase-locked measurements.

The distribution of the coefficient has quite a noticeable error that can be the effect of external light interferences that may have caused some variation in the coefficient. This may have occurred because the signal was not phase-locked to the illumination light or the

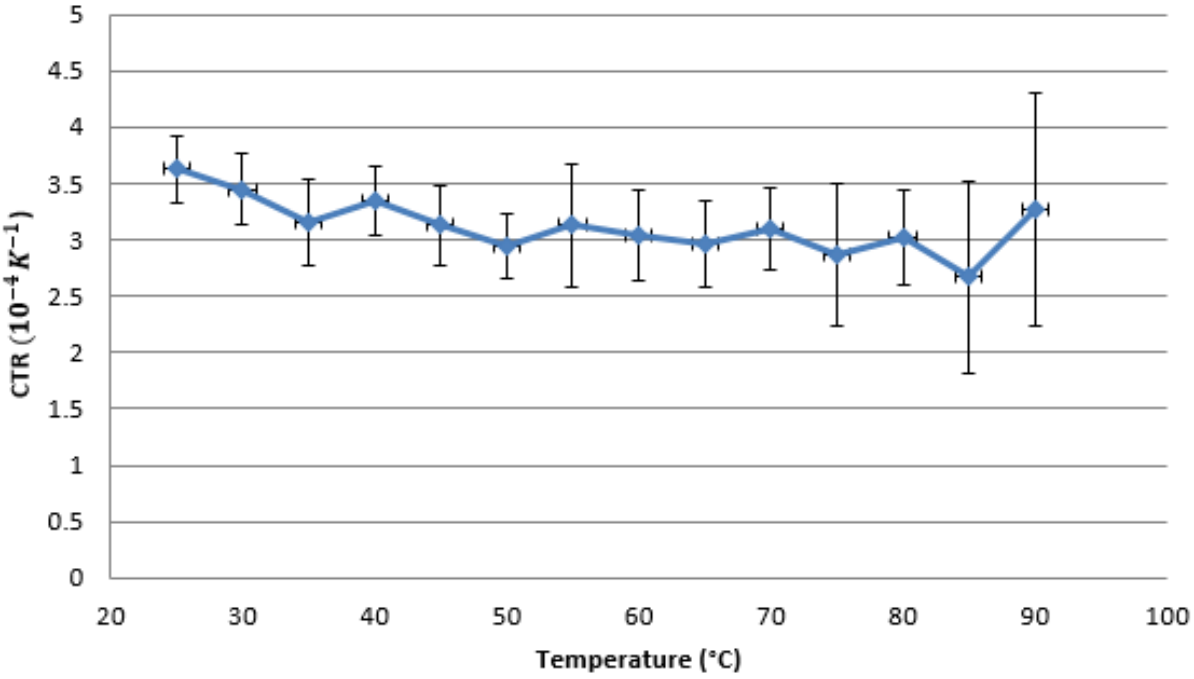

Figure 4.4. Coefficient Variation with Temperature measured with CCD setup

heating process. Moreover, the added alignment and focusing may have counteracted the large thermal expansions and shifts of the sample. This might lead to misalignments and different focusing levels especially that the sample is pure gold and does not contain many features for the alignment and focusing. Other sources of error may be some remaining convective currents that are seen at 85°C and 90°C. These effects may lead to a fluctuating variation in the optical path of light because of the mixing of hot and cold plumes of different refractive indexes.

The uncertainties and added complexities that accompany the alignment, focusing and convective mitigation processes can be avoided by using localized self-heating without the need to heat the whole stage as shown in the next section.

4.4. In-Situ Results

Initial identification of the thermal coefficients of resistance and power coefficient of resistance were performed on the resistor of choice. Preliminary tests determined the best resistor size to use for the tests. To achieve the desired maximum temperature of 100°C, the 20 um resistor required an electric current exceeding 200 mA which rendered the micro-probes contact unstable and unreliable. Under a magnification of 50×, the 5 um and 3 um resistors did not provide enough area to observe and collect intensity frames with the CCD camera. Thus the 10 um resistor was chosen for the calculations having enough pixels for the intensity measurements and with current values not exceeding 130 mA.

4.4.1. Thermal Coefficient of Resistance

The thermal coefficient of resistance was obtained by fitting the relative electrical resistance change to the change in temperature. A linear regression study according to Eq. 3.6 was performed to obtain the coefficient α. The linear relation is shown in Fig. 4.5.

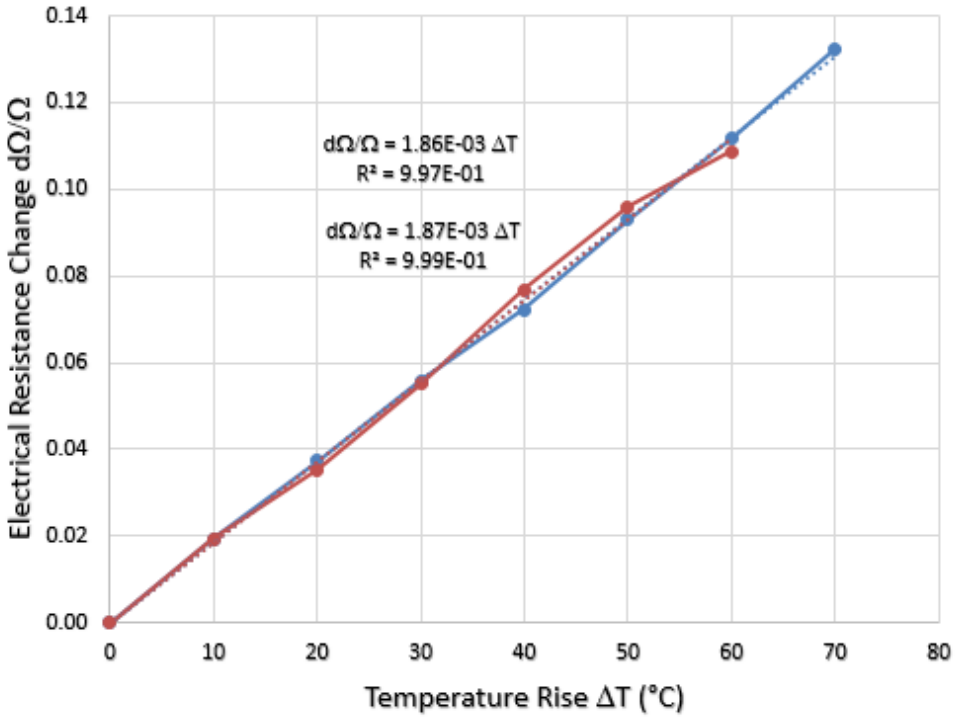

Figure 4.5. Electrical Resistance Change with Temperature Rise

The two curves are for two runs, one with increments of 10°C from the base temperature of 20°C, and another starting at 25°C. The two curves follow a linear increase with temperature at the same rate of $\alpha = 1.87 \times 10^{-3} K^{-1}$ with a standard deviation of $\sigma_\alpha = 2.02 \times 10^{-5} K^{-1}$.

4.4.2. Power Coefficient of Resistance

The power coefficient of resistance was first preliminarily tested to obtain a rough value and estimate a max temperature rise. The base temperature was fixed at 20°C and using the DC Source/Monitor unit, different voltage levels were applied across the resistor while the current was measured to provide a reading for the resistance and power level.

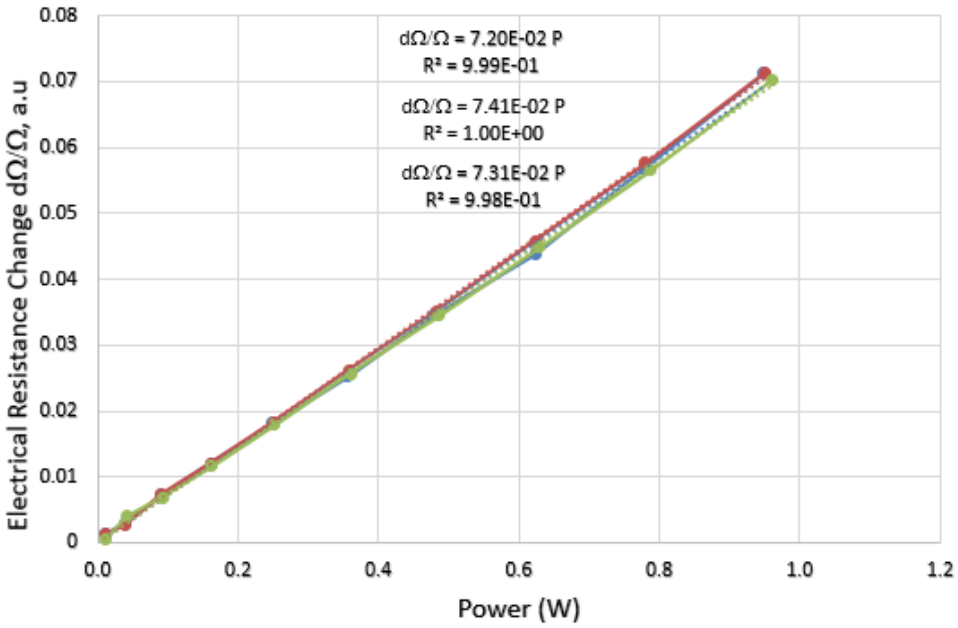

Figure 4.6. Electrical Resistance Change with Power Applied (Preliminary Tests)

The obtained β value used for the calculation of the approximate maximum temperature rise was used also to choose the suitable resistor that would provide sufficient self heating with minimal electric current. From the preliminary run, the power levels were calculated for the needed temperature rises between 0 and 80°C with steps of 10°C.

During the activation of the resistors with constant voltage to the required power level, the current was also monitored and the power-resistance relation was obtained to relate the electrical activation data with the intensity frames. The final value of β used for C_{TR} was derived from the distribution obtained at the time of the activation and frame acquisition to be $\beta = 7.75 \times 10^{-3} W^{-1}$ with a standard deviation of $\sigma_\beta = 5.23 \times 10^{-4} W^{-1}$. The actual power as well as the fluctuations in current values are also recorded during the frames acquisition and the actual temperature is calculated and used for the C_{TR} values as seen in Table 4.1.

Table 4.1. Activation levels for microresistor with calculated actual power and temperature

Temperature Required (°C)	**Power Required (mW)**	**Set Voltage (V)**	**Measured Current (mA)**	**Actual Power (mW)**	**Actual Temperature (°C)**
20	0	0	0	0.00	20.00
30	241	4.95	47.974	237.47	29.86
40	482	7.03	67.117	471.83	39.60
50	722	8.7	81.798	711.64	49.56
60	963	10.1	93.095	940.26	59.05
70	1204	11.4	103.640	1181.50	69.07
80	1445	12.5	112.310	1403.88	78.31
90	1685	13.7	121.370	1662.77	89.06
100	1926	14.8	129.180	1911.86	99.40

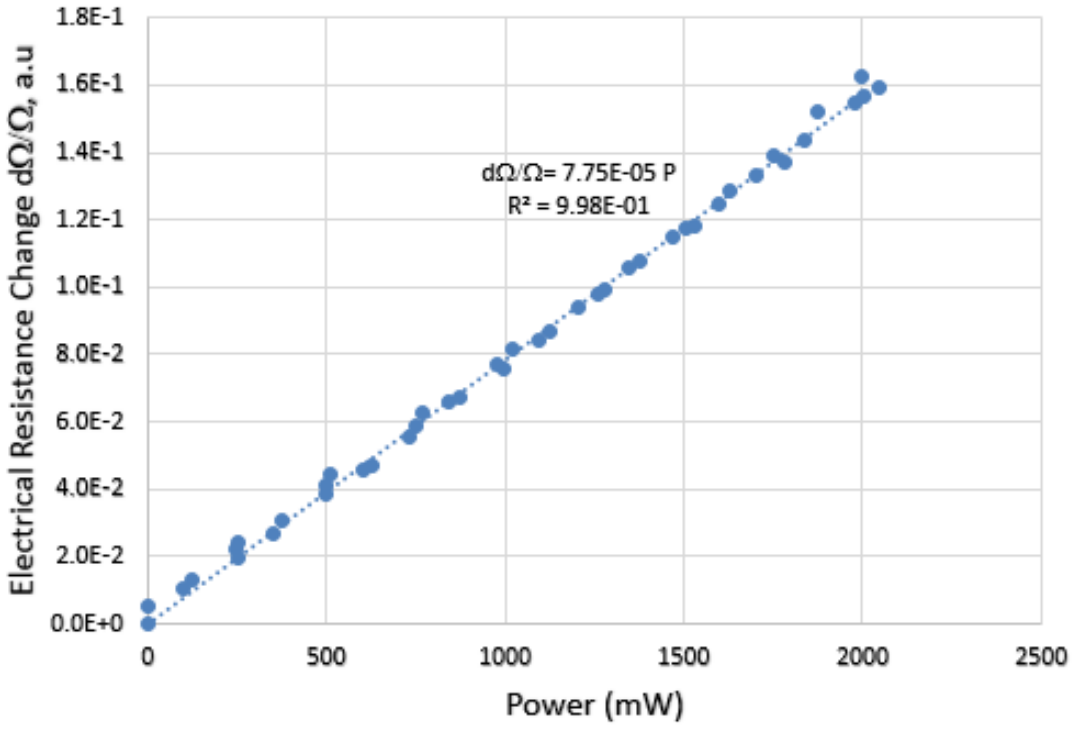

Figure 4.7. Electrical Resistance Change with Power Applied (Activation Run)

4.4.3. Image Post Processing

After acquiring the 200 frames from the CCD camera at each set temperature, a correction was performed with the PD voltage value that is representative of the light source intensity. The correction of the frame intensities is done proportionally with the change of the PD voltage from the average as follows.

$$R_{corrected} = R_i \times \frac{V_{PD_average}}{V_{PD_i}} \tag{4.2}$$

In the phase-locked PD measurements, the correction for source fluctuations is automatically obtained by the differential nature of the PD values since the two photo-detectors had the same sensitivity and amplification. Any fluctuation in the reflected light due to a drift in the source intensity is immediately detected in both PDs and omitted by the differential acquisition.

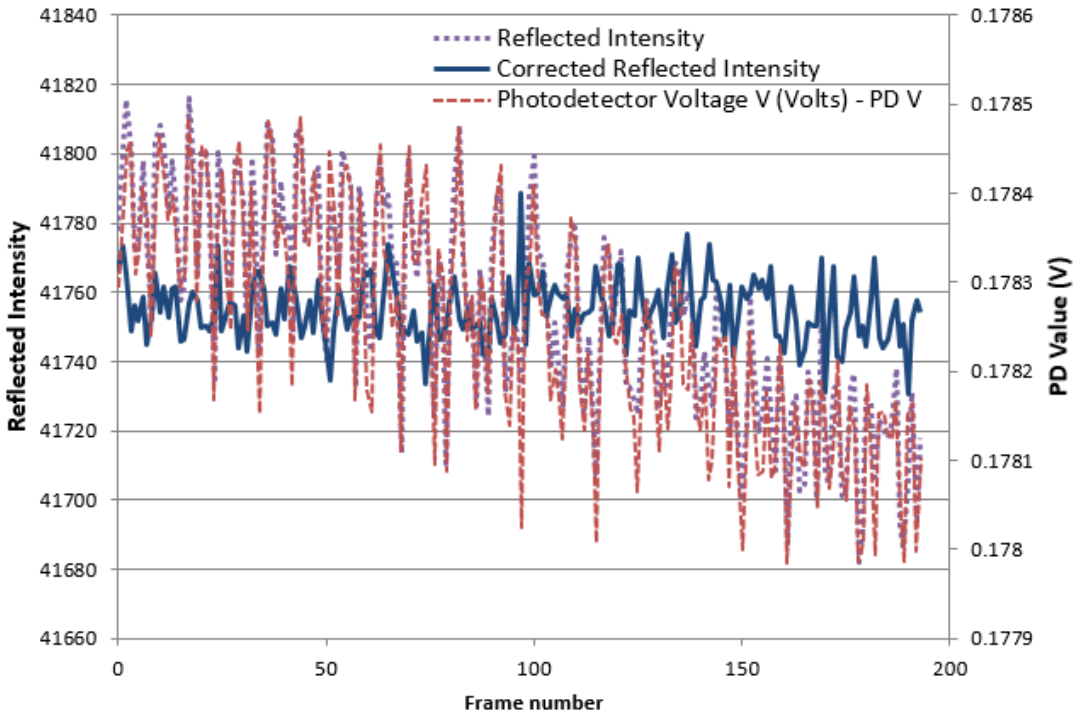

Figure 4.8. Reflected intensity and source-sampling PD value for 200 frames at one temperature level

The correction for a 200 frames set at a prescribed temperature is shown in Fig. 4.8. The correction is done with the average of all frames corresponding to a fixed temperature, which is then used to correct the different PD values for the sets at other temperature levels using the same Eq. 4.2. This ensures that the source fluctuations are stabilized to the same intensity for all frames and sets; any reflection variation is due to the thermoreflectance effect. Figure 4.9 shows the reflected intensities at the measured temperatures as well as the average PD values, and the final corrected intensity temperature curve. It is evident that the correction enhances the signal and reduces the noise.

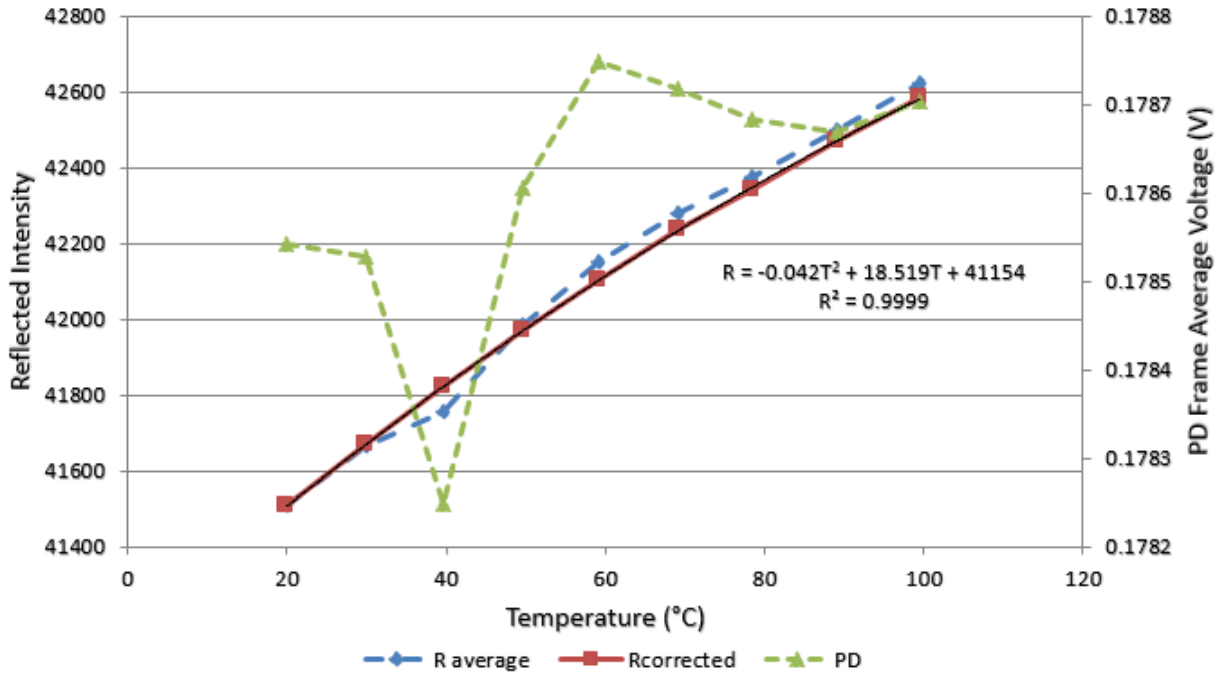

Figure 4.9. Average reflected intensity and source-sampling PD value at each temperature level

4.4.4. Error Analysis

To be able to quantify the error incorporated in the calculation of C_{TR} values, the error of each of the parameters contained in Eq. 3.9 are evaluated. The sources of uncertainties are the activation current, the parameters α and β, and the light reflection intensity R. The errors in the photodetecter sampling the light source and the camera noise errors are all incorporated in the final corrected reflected intensity distribution and reported as an uncertainty in the value of the average reflected intensity. The general expression for C_{TR} used is given in the form of Eq. 4.3.

$$C_{TR} = \left(\frac{R_{T_2}}{R_{T_1}} - 1\right) \times \left[\frac{\beta}{\alpha} \times (U_2 I_2 - U_1 I_1)\right]^{-1} \tag{4.3}$$
$$C_{TR} = \Delta R^* \times \left(\frac{\beta}{\alpha} \times \Delta P\right)^{-1}$$

The uncertainty analysis for an experimental study with multiple primary variables has been presented by Kline and McClintock [11]. The uncertainty w_F for a variable F which is a function of n independent variables $x_1, x_2, x_3, ...x_n$ having the uncertainties $w_1, w_2, w_3, ...w_n$ is presented by

$$w_F = \sqrt{\sum_{i=1}^{n} \left(\frac{\partial F}{\partial x_i} w_i\right)^2} \tag{4.4}$$

For our case, the uncertainty in the value of the C_{TR} is due to the propagation of error from the values of R, P, β and α. The parameters are assumed as independent and random for Eq. 4.4 to hold [22]. The first uncertainty is obtained from the current reading from the source monitor unit for the constant voltage applied over the duration of frame acquisitions. The uncertainty in the reflected intensity values is calculated for a set of acquired frames that is post processed by cleansing pixels with impurities and correcting the average for source fluctuations and drift using the source-sampling photodetector. The calibration fits

for α and β also provide the errors on the slope in the linear regression shown in Eq. 4.5a.

$$\sigma_{\alpha,\beta} = \sigma_y \sqrt{\frac{\Sigma x^2}{\Delta}} \tag{4.5a}$$

$$\Delta = N\Sigma x^2 - (\Sigma x)^2 \tag{4.5b}$$

The expression for the partial derivatives of C_{TR} with respect to the independent variables and the expressions for their uncertainties are shown as follows in Eq. 4.6.

$$w_{\Delta R^*} = \left| \frac{R_{T_2}}{R_{T_1}} - 1 \right| \sqrt{\left(\frac{w_{R_{T2}}}{R_{T2}}\right)^2 + \left(\frac{w_{R_{T1}}}{R_{T1}}\right)^2} \tag{4.6a}$$

$$w_{\Delta P} = U_1 \times w_{I_1} + U_2 \times w_{I_2} \tag{4.6b}$$

Finally, the error on the C_{TR} value is given in terms of the independent variables and their uncertainties according the propagation of error equation for products and quotients Eq. 4.7.

$$\frac{w_{C_{TR}}}{C_{TR}} = \sqrt{\left(\frac{w_{\Delta P}}{\Delta P}\right)^2 + \left(\frac{w_{\Delta R^*}}{\Delta R^*}\right)^2 + \left(\frac{w_{\beta/\alpha}}{\beta/\alpha}\right)^2} \tag{4.7}$$

The variation of the calculated C_{TR} coefficients from the reflectance temperature scale is shown in Fig.4.10. The results of the C_{TR} dependence on temperature show a similar decreasing trend from around $3.7{\times}10^{-4}K^{-1}$ at 25°C to $2.5{\times}10^{-4}K^{-1}$. The results match the behavior observed with the other calibration setups and show that the linear assumption does not hold for all temperatures. The errors were less pronounced for this method mainly due to localized heating and insignificant thermal expansion. The discrepancy between the calibration results is partially because the samples are different and the magnification used is 50×, compared to a 20× for the phase-locked PD setup, to acquire enough intensity readings within the width of the gold microresistor.

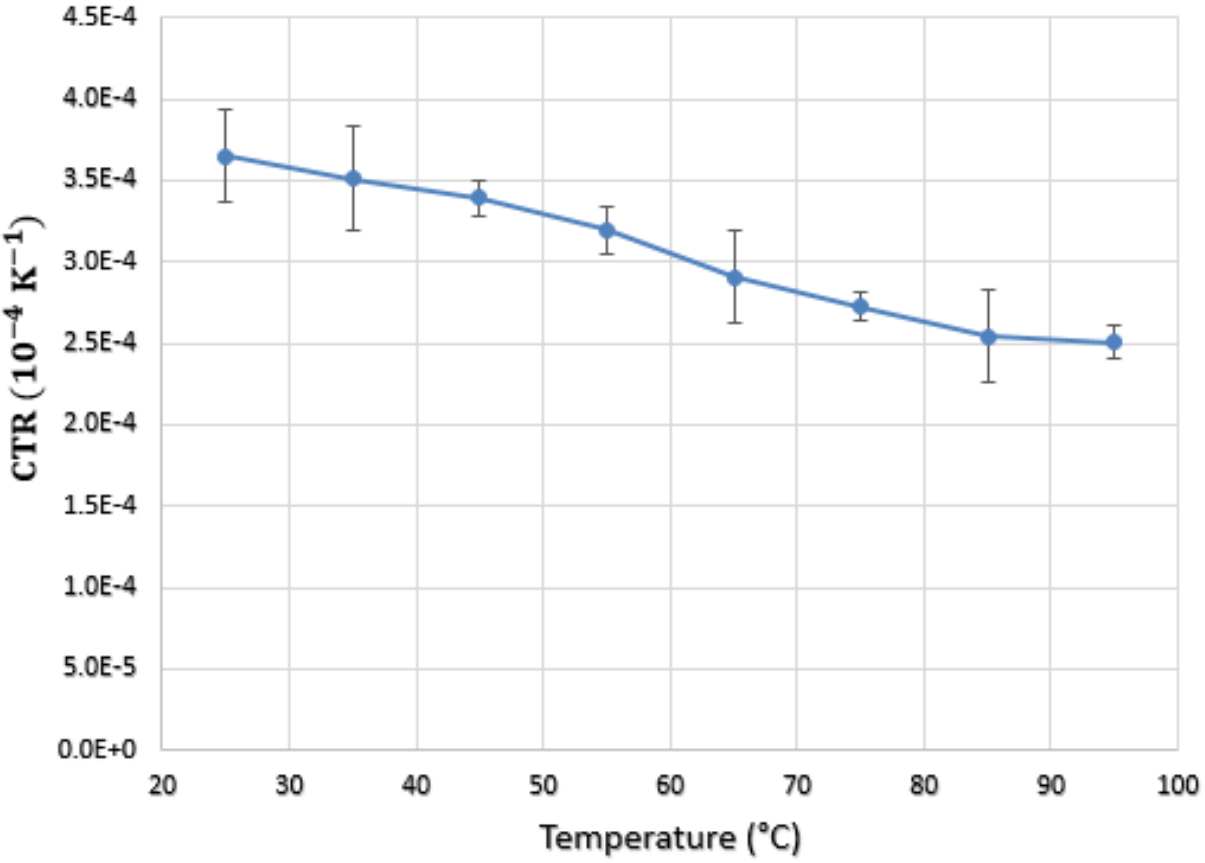

Figure 4.10. Coefficient of Thermoreflectance obtained with self-heating CCD setup

Chapter 5

CONCLUSIONS

Thermoreflectance has been proven to be a fast and reliable thermography technique that can be used for measuring temperature maps at the spatial microscales as well as measuring other thermal properties of microelectronic structures. However, the thermal reflectance variation signal is on the order of 0.1% per degree, which may render the optical effect difficult to detect, and the corresponding temperature maps more tedious to identify. Moreover, the signal is dependent on the sample, the wavelength of light, and the optical path, which requires calibration before every measurement to identify the reflectance temperature relation for the sample. In this study, the importance of the calibration procedure on the accuracy of the measurements are identified by measuring the thermal reflectance coefficient and assessing its variation across the temperature spectrum between 25°C and 100°C. Different calibration methods were performed and compared regarding their precision and applicability. A phase-locked differential calibration setup investigated the linear assumption of the TR relation and found a weak second-order effect that would be otherwise dominated by the instrumental noise. Even though these effects are minimal compared to the dominant first order terms, a drop of 25% in the C_{TR} value led to an error in the accuracy in excess of 10°C which is 10% of the full temperature range.

In applications where the thermography technique is used for locating hot spots and assessing designs of structures and heat spreaders, the added temperature accuracy is not crucial. However, if used to measure failure temperatures or if used with computational engines for thermal characterization, special care should be given to the drifts from the linear behavior. In pump and probe methods, it is sufficient to ensure that the maximum temperature rise does not increase greatly so that the linear assumption can be valid. For high power devices, more complex calibration is needed to attain a better accuracy where

the signal could be enhanced using phase-locked measurements and vacuum isolation for temperatures exceeding 100°C. In all cases, it is essential that the calibration conditions be identical to those of the activation setup which adds also some complexities to measure in thermally controlled chambers.

The thermoreflectance effects is the result of complex physics and involves the combined effects of temperature on the interaction between the energy of the incident photon and the surface lattice energy structure. The overall effect can be characterized by a dependency of the C_{TR} on wavelength and temperature for a given material. The change in C_{TR} could be presented as a shift in the wavelength distribution of Section 4.1. The study can be extended for different conducting materials used in micro-fabrication (Aluminum, Copper and Platinum), and a generalized C_{TR} dependence on the wavelength and temperature can be formulated. This would give researchers an idea of the temperature shifts for different wavelength, and could present wavelengths for higher accuracy measurements where C_{TR} is less sensitive to temperature.

BIBLIOGRAPHY

[1] Abeles, F. *Optical properties of solids*. North-Holland Pub. Co, Amsterdam;New York;, 1972.

[2] Burzo, M. G., Komarov, P. L., and Raad, P. E. Noncontact transient temperature mapping of active electronic devices using the thermoreflectance method. *IEEE Transactions on Components and Packaging Technologies 28*, 4 (Dec 2005), 637–643.

[3] Burzo, M. G., Komarov, P. L., and Raad, P. E. Optimized thermo-reflectance system for measuring the thermal properties of thin-films and their interfaces. In *Twenty-Second Annual IEEE Semiconductor Thermal Measurement And Management Symposium* (March 2006), pp. 87–94.

[4] Burzo, M. G., Komarov, P. L., and Raad, P. E. Pixel-by-pixel calibration of a ccd camera based thermoreflectance thermography system with nanometer resolution. In *2009 15th International Workshop on Thermal Investigations of ICs and Systems* (Oct 2009), pp. 130–135.

[5] Burzo, M. G., Raad, P. E., Lee, T., and Komarov, P. L. Thermal conductivity measurements of novel SOI films using submicron thermography and transient thermoreflectance. In *2012 28th Annual IEEE Semiconductor Thermal Measurement and Management Symposium (SEMI-THERM)* (March 2012), pp. 150–156.

[6] Christofferson, J., Maize, K., Ezzahri, Y., Shabani, J., Wang, X., and Shakouri, A. Microscale and nanoscale thermal characterization techniques. In *2007 International Conference on Thermal Issues in Emerging Technologies: Theory and Application* (Jan 2007), pp. 3–9.

[7] Farzaneh, M., Maize, K., Leren, D., Summers, J. A., Mayer, P. M., Raad, P. E., Pipe, K. P., Shakouri, A., Ram, R. J., and Hudgings, J. A. CCD-based thermoreflectance microscopy: principles and applications. *Journal of Physics D: Applied Physics 42*, 14 (2009), 143001.

[8] Favaloro, T., Bahk, J.-H., and Shakouri, A. Characterization of the temperature dependence of the thermoreflectance coefficient for conductive thin films. *Review of Scientific Instruments 86*, 2 (2015), 024903.

[9] Grauby, S., Dilhaire, S., Jorez, S., and Claeys, W. Temperature variation mapping of a microelectromechanical system by thermoreflectance imaging. *IEEE Electron Device Letters 26*, 2 (Feb 2005), 78–80.

[10] Hatta, I. Thermal diffusivity measurements of thin films and multiulayered composites. *International Journal of Thermophysics* (1990).

[11] Kline, S. J., and McClintock, F. A. Describing the uncertainties in single sample experiments. *Mechanical Engineering* ((1953).), 38.

[12] Komarov, P. L., Burzo, M. G., and Raad, P. E. A thermoreflectance thermography system for measuring the transient surface temperature field of activated electronic devices. In *Twenty-Second Annual IEEE Semiconductor Thermal Measurement And Management Symposium* (March 2006), pp. 199–203.

[13] Liu, Y., Mandelis, A., Choy, M., Wang, C., and Segal, L. Remote quantitative temperature and thickness measurements of plasma-deposited titanium nitride thin coatings on steel using a laser interferometric thermoreflectance optical thermometer. *Review of Scientific Instruments 76*, 8 (2005), 084902.

[14] Pop, E., and Goodson, K. Thermal phenomena in nanoscale transistors (reprinted from the IEEE ITHERM 2004 proceedings - the ninth intersociety conference on thermal and thermomechanical phenomena in electronic systems, june 1-4, 2004, las vegas, nv usa). *Journal OF Electronic Packaging 128*, 2 (2006), 102–108.

[15] Raad, P. E., Burzo, M. G., and Komarov, P. L. Numerical simulation of complex submicron devices with experimentally determined power maps. In *2009 15th International Workshop on Thermal Investigations of ICs and Systems* (Oct 2009), pp. 36–39.

[16] Raad, P. E., Komarov, P. L., and Burzo, M. G. Coupling surface temperature scanning and ultra-fast adaptive computing to thermally fully characterize complex three-dimensional electronic devices. In *Twenty-Second Annual IEEE Semiconductor Thermal Measurement And Management Symposium* (March 2006), pp. 204–209.

[17] Reddy, H., Guler, U., Kildishev, A. V., Boltasseva, A., and Shalaev, V. M. Temperature-dependent optical properties of gold thin films. *Opt. Mater. Express 6*, 9 (Sep 2016), 2776–2802.

[18] Rosei, R., and Lynch, D. W. Thermomodulation spectra of Al, Au and Cu. *Physical Review B 5*, 10 (1972), 3883–3894.

[19] Schlag, R., Ras, M. A., Arlt, V., May, D., Winkler, T., and Wunderle, B. Precision determination of thermoreflectance coefficients for localised thermometry. In *2015 21st International Workshop on Thermal Investigations of ICs and Systems (THERMINIC)* (Sept 2015), pp. 1–5.

[20] Seraphin, B. O., and Bottka, N. Band-structure analysis from electro-reflectance studies. *Phys. Rev. 145* (May 1966), 628–636.

[21] SINGH, Y. Electrical resistivity measurements: A review. *International Journal of Modern Physics: Conference Series 22* (2013), 745–756.

[22] Taylor, J. R. *An Introduction To Error Analysis*. 1997.

[23] Tessier, G., Pavageau, S., Charlot, B., Filloy, C., Fournier, D., Cretin, B., Dilhaire, S., Gomes, S., Trannoy, N., Vairac, P., and Volz, S. Quantitative thermoreflectance imaging: Calibration method and validation on a dedicated integrated circuit. *IEEE Transactions on Components and Packaging Technologies 30*, 4 (Dec 2007), 604–608.